Eur. Phys. J. Special Topics **143**, 181–189 (2007)

DOI: 10.1140/epjst/e2007-00086-x

THE EUROPEAN PHYSICAL JOURNAL
SPECIAL TOPICS

Particles in fluids

H.J. Herrmann[1,2], J.S. Andrade Jr.[2], A.D. Araújo[2], and M.P. Almeida[2]

[1] IfB, ETH Zürich, Hönggerberg, 8093 Zürich, Switzerland
[2] Departamento de Física, Universidade Federal do Ceará, 60451-970 Fortaleza, Ceará, Brazil

Abstract. For finite Reynolds numbers the interaction of moving fluids with particles is still only understood phenomenologically. We will present three different numerical studies all using the solver "Fluent" which elucidate this issue from different points of view. On one hand we will consider the case of fixed particles, i.e. a porous medium and present the distribution of channel openings and fluxes. These distributions show a scaling law in the density of particles and for the fluxes follow an unexpected stretched exponential behaviour. The next issue will be filtering, i.e. the release of massive tracer particles within this fluid. Interestingly a critical Stokes number below which no particles are captured and which is characterized by a critical exponent of 1/2. Finally we will also show data on saltation, i.e. the motion of particles on a surface which dragged by the fluid performs jumps. This is the classical aeolian transport mechanism responsible for dune formation. The empirical relations between flux and wind velocity are reproduced.

1 Introduction

Particles in fluids (liquids or gases) appear in many applications in chemical engineering, fluid mechanics, geology and biology [1–3]. Also fluid flow through a porous medium is of importance in many practical situations ranging from oil recovery to chemical reactors and has been studied experimentally and theoretically for a long time [4–6]. Due to disorder, porous media display many interesting properties that are however difficult to handle even numerically. One important feature is the presence of heterogeneities in the flux intensities due the varying channel widths. They are crucial to understand stagnation, filtering, dispersion and tracer diffusion.

In the porous space the fluid mechanics is based on the assumption that a Newtonian and incompressible fluid flows under steady-state conditions. We consider the Navier-Stokes and continuity equations for the local velocity $\vec{u}$ and pressure fields p, being ρ the density of the fluid. No-slip boundary conditions are applied along the entire solid-fluid interface, whereas a uniform velocity profile, $u_x(0, y) = V$ and $u_y(0, y) = 0$, is imposed at the inlet of the channel. For simplicity, we restrict our study to the case where the Reynolds number, defined here as $Re \equiv \rho V L_y/\mu$, is sufficiently low ($Re < 1$) to ensure a laminar viscous regime for fluid flow. We use FLUENT [7], a computational fluid dynamic solver, to obtain the numerical solution on a triangulated grid of up to hundred thousand points adapted to the geometry of the porous medium.

The investigation of single-phase fluid flow at low Reynolds number in disordered porous media is typically performed using Darcy's law [4,6], which assumes that a *macroscopic* index, the permeability K, relates the average fluid velocity V through the pores with the pressure drop ΔP measured across the system,

$$V = -\frac{K}{\mu}\frac{\Delta P}{L} , \tag{1.1}$$

where L is the length of the sample in the flow direction and μ is the viscosity of the fluid. In previous studies [9–15], computational simulations based on detailed models of pore geometry and fluid flow have been used to predict permeability coefficients.

Here we present numerical calculations for a fluid flowing through a two-dimensional channel of width L_y and length L_x filled with randomly positioned circular obstacles [16]. For instance, this type of model has been frequently used to study flow through fibrous filters [27]. Here the fluid flows in the x-direction at low but non-zero Reynolds number and in the y-direction we impose periodic boundary conditions. We consider a particular type of random sequential adsorption (RSA) model [18] in two dimensions to describe the geometry of the porous medium. As shown in Fig. 1, disks of diameter D are placed randomly by first choosing from a homogeneous distribution between $D/2$ and $L_x - D/2$ ($L_y - D/2$) the random x-(y-)coordinates of their center. If the disk allocated at this position is separated by a distance smaller than $D/10$ or overlaps with an already existing disk, this attempt of placing a disk is rejected and a new attempt is made. Each successful placing constitutes a decrease in the porosity (void fraction) ϵ by $\pi D^2/4L_xL_y$. One can associate this filling procedure to a temporal evolution and identify a successful placing of a disk as one time step. By stopping this procedure when a certain value of ϵ is achieved, we can produce in this way systems of well controlled porosity. We study in particular configurations with $\epsilon = 0.6$, 0.7, 0.8 and 0.9.

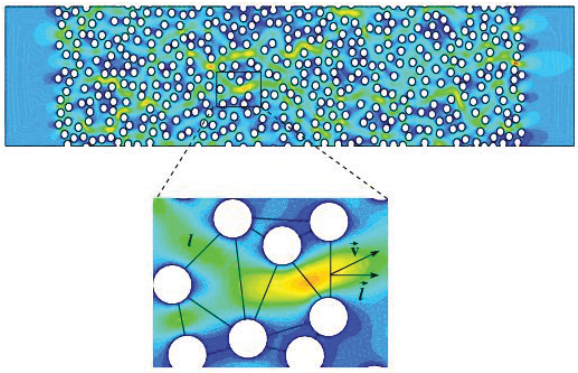

Fig. 1. Velocity magnitude for a typical realization of a pore space with porosity $\epsilon = 0.7$ subjected to a low Reynolds number and periodic boundary conditions applied in the y-direction. The fluid is pushed from left to right. The colors ranging from blue (dark) to red (light) correspond to low and high velocity magnitudes, respectively. The close-up shows a typical pore opening of length l across which the fluid flows with a line average velocity $\vec{v}$. The local flux at the pore opening is given by $q = vl\cos\theta$, where θ is the angle between $\vec{v}$ and the vector normal to the line connecting the two disks.

2 Various distributions in porous medium

The geometry of our random configurations can be analyzed making a Voronoi construction of the point set given by the centers of the disks [19,20]. We define two disks to be neighbors of each other if they are connected by a bond of the Voronoi tessellation. These bonds constitute therefore the openings or pore channels through which a fluid can flow when it is pushed through our porous medium, as can be seen in the close-up of Fig. 1. We measure the channel widths l as the length of these bonds minus the diameter D and plot in Fig. 2 the (normalized) distributions of the normalized channel widths $l^* = l/D$ for the four different porosities. Clearly one notices two distinct regimes: (*i*) for large widths l^* the distribution decays seemingly exponentially with l^*, and (*ii*) for small l^* it has a strong dependence on the porosity, increasing with decreasing porosity dramatically at the origin. Between the two regimes a crossover is visible as a peak which shifts between $\epsilon = 0.9$ and 0.8 and then stays for smaller porosities at about $l^* = 1$, i.e., $l = D$.

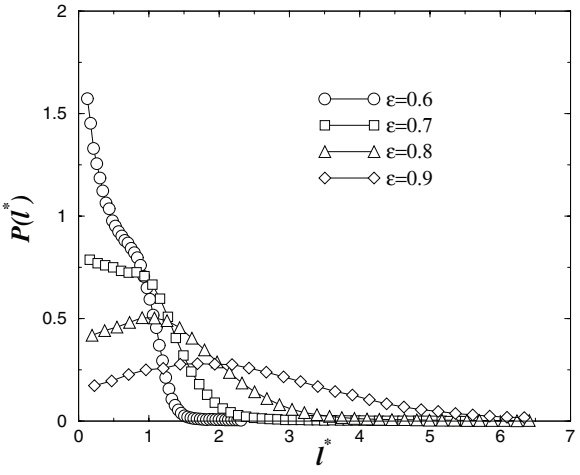

Fig. 2. The distributions of the normalized channel widths $l^* = l/D$ for different values of porosity ϵ. From left to right, the two vertical dashed lines indicate the values of the minimum distance between disks $l^* = 0.1$ and the size of the disks $l^* = 1$.

Let us now analyse the distribution of fluxes throughout the porous medium. Each local flux q crossing its corresponding pore opening l is given by $q = vl\cos\theta$, where θ is the angle between $\boldsymbol{v}$ and the vector normal to the cross section of the channel (see Fig. 1). In Fig. 3 we show that the distributions of normalized fluxes $\phi = q/q_t$, where $q_t = VL_y$ is the total flux, have a stretched exponential form, $P(\phi) \sim \exp(-\sqrt{\phi/\phi_0})$, with $\phi_0 \approx 0.005$ being a characteristic value. This simple form is quite unexpected considering the rather complex dependence of $P(l)$ on ϵ. Moreover, all flux distributions $P(\phi)$ collapse on top of each other when rescaled by the corresponding value of $\langle l^* \rangle^{-1} \epsilon^2$. This collapse for distinct porous media results from the fact that mass conservation is imposed at the microscopic level of the geometrical model adopted here, which is microscopically disordered, but is macroscopically homogeneous at a larger scale [6].

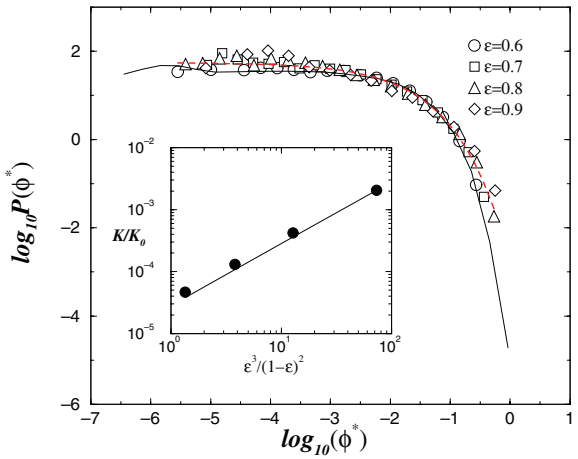

Fig. 3. The log-log plot of the distributions of the normalized local fluxes $\phi = q/q_t$ for different porosities ϵ. The (red) dashed line is a fit of the form $\exp(-\sqrt{\phi/\phi_0})$, where $\phi_0 \approx 0.005$. In the inset we see a double-logarithmic plot of the global flux and the straight line verifies the Kozeny-Carman equation.

3 Results on filtration

Filtration is typically used to get clean air or water and also plays a crucial role in the chemical industry. For this reason it has been studied extensively in the past [21]. In particular, we will focus here on deep bed filtration where the particles in suspension are much smaller than the pores of the filter which they penetrate until being captured at various depths. For

non-Brownian particles, at least four capture mechanisms can be distinguished, namely, the geometrical, the chemical, the gravitational and the hydrodynamical one [21].

Very carefully controlled laboratory experiments were conducted in the past by Ghidaglia *et al.* [22] evidencing a sharp transition in particle capture as function of the dimensionless ratio of particle to pore diameter characterized by the divergence of the penetration depth. Subsequently, Lee and Koplik [23] found a transition from an open to a clogged state of the porous medium that is function of the mean particle size. Much less effort, however, has been dedicated to quantify the effect of inertial impact on the efficiency of a deep bed filter.

Here we will concentrate on the inertial effects in capture which constitute an important mechanism in most practical cases and, despite much effort, are quantitatively not yet understood, as reviewed in Ref. [24]. The effect of inertia on the suspended particles is usually quantified by the dimensionless *Stokes number*, $St \equiv V d_p^2 \rho_p / 18 \ell \mu$, where d_p and ρ_p are the diameter and density of the particle, respectively, ℓ is a characteristic length of the pores, μ is the viscosity and V is the velocity of the fluid. Inertial capture by fixed bodies has already been described since 1940 by Taylor and proven to happen for inviscid fluids above a critical Stokes number [25]. It is our aim to present a detailed hydrodynamic calculation of the inertial capture of particles in a porous medium. We will disclose novel scaling relations.

Let us first consider the case of an infinite ordered porous medium composed of a periodic arrangement of fixed circular obstacles (e.g., cylinders) [26]. This system can then be completely represented in terms of a single square cell of unitary size and porosity given by $\epsilon \equiv (1 - \pi D^2/4)$, where D is the diameter of the obstacle, as shown in Fig. 4. Assuming Stokesian flow through the void space an analytical solution has been provided by Marshall *et al.* [27]. Here we use this solution to obtain the velocity flow field $\mathbf{u}$ and study the transport of particles numerically. For simplicity, we assume that the influx of suspended particles is so small that (*i*) the fluid phase is not affected by changes in the particle volume fraction, and (*ii*) particle-particle interactions are negligible. Moreover, we also consider that the movement of the particles does not impart momentum to the flow field. Finally, if we assume that the drag force and gravity are the only relevant forces acting on the particles, their trajectories can be calculated by integration of the following equation of motion $\frac{d\mathbf{u}_p^*}{dt^*} = \frac{(\mathbf{u}^* - \mathbf{u}_p^*)}{St} + F_g \frac{\mathbf{g}}{|\mathbf{g}|}$, where $F_g \equiv (\rho_p - \rho)\ell|\mathbf{g}|/(V^2 \rho_p)$ is a dimensionless parameter, $\mathbf{g}$ is gravity, t^* is a dimensionless time, and $\mathbf{u}_p^*$ and $\mathbf{u}^*$ are the dimensionless velocities of the particle and the fluid, respectively.

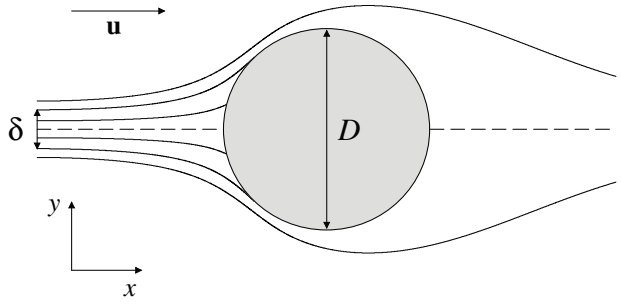

Fig. 4. The trajectories of particles released from different positions at the inlet of the periodic porous medium cell. $St = 0.25$ and the flow field $\mathbf{u}$ is calculated from the analytical solution of Marshall *et al.* [27]. The thick solid lines correspond to the limiting trajectories that determine δ.

We show in Fig. 4 some trajectories calculated for particles released in the flow for $St = 0.25$. Once a particle touches the boundary of the obstacle, it gets trapped. Our objective here is to search for the position y_0 of release at the inlet of the unit cell ($x_0 = 0$) and above the horizontal axis (the dashed line in Fig. 4), below which the particle is always captured and above which the particle can always escape from the system. As depicted in Fig. 4, the particle capture efficiency can be straightforwardly defined as $\delta \equiv 2y_0$. In the limiting case where $St \to \infty$, since the particles move ballistically towards the obstacle, the particle efficiency reaches its

maximum, $\delta = D$. For $St \to 0$, on the other hand, the efficiency is smallest, $\delta = 0$. In this last situation, the particles can be considered as tracers that follow exactly the streamlines of the flow and are therefore not trapped.

We show in Fig. 5 the log-log plot of the variation of δ/D with the rescaled Stokes number in the presence of gravity for three different porosities. In all cases, the variable δ increases linearly with St to subsequently reach a crossover at $St_\times$, and finally approach its upper limit ($\delta = D$). The results of our simulations also show that $St_\times \sim (\epsilon - \epsilon_{min})$, where ϵ_{min} corresponds to the minimum porosity below which the distance between inlet and obstacle is too small for a massive particle to deviate from the obstacle. The collapse of all data shown in Fig. 5 confirms the validity of the scaling law.

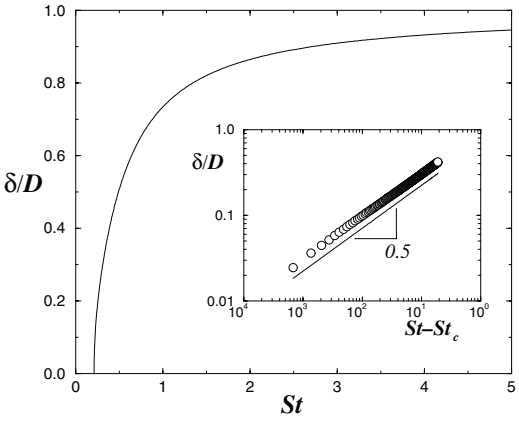

Fig. 5. The dependence of the capture efficiency δ on the rescaled Stokes number $St/(\epsilon - \epsilon_{min})$ for periodic porous media in the presence of gravity. Here we use $F_g = 16$, a value that is compatible with the experimental setup described in Ref. [22]. The inset shows that the behavior of the system without gravity can be characterized as a second order transition, $\delta \sim (St - St_c)^\alpha$, with $\alpha \approx 0.5$ and $St_c = 0.2679 \pm 0.0001$, 0.2096 ± 0.0001 and 0.1641 ± 0.0001, for $\epsilon = 0.85$, 0.9 and 0.95, respectively.

We see in the inset of Fig. 5 that the behavior of the system in terms of particle capture becomes significantly different in the absence of gravity. The efficiency δ remains equal to zero up to a certain critical Stokes number, St_c, that corresponds to the maximum value of St below which particles cannot be captured, regardless of the position y_0 at which they have been released. Right above St_c, the variation of δ can be described in terms of a power-law, $\delta \sim (St - St_c)^\alpha$, with an exponent $\alpha \approx 0.5$. Our results show that, while the exponent α is practically independent of the porosity for $\epsilon > 0.8$, the critical Stokes number decreases with ϵ, and therefore with the distance from the obstacle where the particle is released (see Fig. 5). To our knowledge, this behavior, that is typical of a second order transition, has never been reported before for inertial capture of particles. In order to have a more realistic model for the porous structure we did also include disorder [26]. Here we adopted a random pore space geometry [18] shown in Fig. 1 and obtained the same results as for the regular case.

4 The mechanism of saltation

Aeolian of sand is a major factor in sand encroachment, dune motion and the formation of coastal and desert landscapes. The dominating transport mechanism is saltation as first described by Bagnold [28] which consists of grains being ejected upwards, accelerated by the wind and finally impacting onto the ground producing a splash of new ejected particles. Reviews are given in Refs. [29,30]. A quantitative understanding of this process is however not achieved.

The wind loses more momentum with increasing number of airborne particles due to Newton's second law until a saturation is reached. The maximum number of grains a wind of given strength can carry through a unit area per unit time defines the saturated flux of sand q_s. This quantity has been measured by many authors in wind tunnel experiments and on the field, and numerous empirical expressions for its dependence on the strength of the wind have been proposed [31,32]. In previous studies theoretical forms have also been derived using

approximations for the drag in turbulent flow [33,34]. All these relations are expressed as polynomials in the wind shear velocity u_* which are of third order, under the assumption that the grain hopping length scales with u_* [31–35]. The velocity profile in a particle laden layer has also been the object of measurement [36,37] and modellization [38]. The complete analytical treatment of this problem remains out of reach not only because of the turbulent character of the wind, but also due to the underlying moving boundary conditions in the equations of motion. More recently, a deterministic model for aeolian sand transport without height dependency in the feedback has been proposed [39]. Despite much research in the past [40] there remain many uncertainties about the trajectories of the particles and their feedback with the velocity field of the wind.

Here we present the first numerical study of saltation which solves the turbulent wind field and its feedback with the dragged particles [41]. As compared to real data, our values have no experimental fluctuations neither in the wind field nor in the particle size. As a consequence, we can determine all quantities with higher precision than ever before, and therefore with a better resolution close to the critical velocity at which grains start to be transported.

To get a quantitative understanding of the layer of airborne particle transport above a granular surface, we simulate the situation inside a two-dimensional channel with a mobile top wall as shown in Fig. 6 schematically.

Here a pressure gradient is imposed between the left and the right side. Gravity points down, i.e., in negative y-direction. The y-dependence of the pressure drop is adjusted in such a way as to insure a logarithmic velocity profile along the entire channel in the case without particles, as it is expected in fully developed turbulence [42]. More precisely, this profile follows the classical form

$$u_x(y) = (u_*/\kappa)\ln(y/y_0)\ , \tag{4.1}$$

where u_x is the component of the wind velocity in the x-direction, u_* is the shear velocity, $\kappa = 0.4$ is the von Karman constant and y_0 is the roughness length which is typically between 10^{-4} and $10^{-2}\,m$. The upper wall of the channel is moved with a velocity equal to the velocity of the wind at that height in order to insure a non-slip boundary condition.

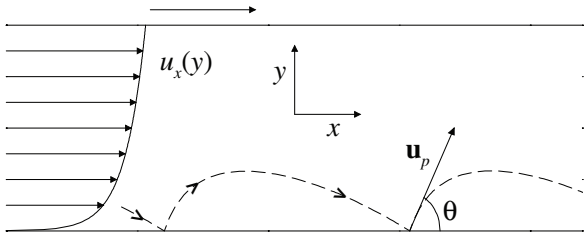

Fig. 6. Setup showing the mobile wall at the top, the velocity field at different positions in the y-direction and the trajectory of a particle stream (dashed line).

Inside the channel we have air flowing under steady-state and homogeneous turbulent conditions. The Reynolds-averaged Navier-Stokes equations with the standard $k-\epsilon$ model are used to describe turbulence. The solution for the velocity and pressure fields is obtained through discretization by means of the control volume finite-difference technique [7].

Having produced a steady-state turbulent flow, we proceed with the simulation of the particle transport along the channel. Assuming that drag and gravity are the only relevant forces acting on the particles, their trajectory can be obtained by integrating the following equation of motion:

$$\frac{d\mathbf{u}_p}{dt} = F_D(\mathbf{u}-\mathbf{u}_p) + \mathbf{g}(\rho_p-\rho)/\rho_p\ , \tag{4.2}$$

where u_p is the particle velocity, $\mathbf{g}$ is gravity and $\rho_p = 2650\ kg\ m^{-3}$ is a typical value for the density of sand particles. The term $F_D(\mathbf{u}-\mathbf{u}_p)$ represents the drag force per unit particle

mass where

$$F_D = \frac{18\mu}{\rho_p d_p^2} \ \frac{C_D \mathrm{Re}}{24} \ , \tag{4.3}$$

$d_p = 2.5 \times 10^{-4}\ m$ is a typical particle diameter, $\mathrm{Re} \equiv \rho d_p \left|\mathbf{u}_p - \mathbf{u}\right| / \mu$ is the particle Reynolds number, and the drag coefficient C_D is taken from empirical relations. Each particle in our calculation represents in fact a stream of real grains. It is necessary to take into account the feedback on the local fluid velocity due to the momentum transfer to and from the particles.

We see in Fig. 6 the trajectory of one particle stream and the velocity vectors along the y-direction. Each time a particle hits the ground it loses a fraction r of its energy and a new stream of particles is ejected at that position with an angle θ. The parameters $r = 0.84$ and $\theta = 36^\circ$ are chosen from experiments [43,44].

We see in Fig. 7 the plot of q_s as function of the wind velocity u_*. Clearly, there exists a critical wind velocity threshold u_t below which no sand transport occurs at all. This agrees well with experimental observations [28,32]. Also shown in Fig. 7 is the best fit to the numerical data using the classical expression proposed by Lettau and Lettau [32],

$$q_s = C_L \frac{\rho}{g} u_*^2 (u_* - u_t) \ , \tag{4.4}$$

where C_L is an adjustable parameter. We find rather good agreement using fit parameters of the same order as those of the original work [32] and a threshold value of $u_t = 0.35 \pm 0.02$. This is in fact, to our knowledge, the first time a numerical calculation is able to quantitatively reproduce this empirical expression and it confirms the validity of our simulation procedure. Other empirical relations from the literature [33–35] can also be used to fit these results. In Fig. 7 we also show that for large values of u_* asymptotically one recovers Bagnold's cubic dependence. Close to the critical velocity u_t interestingly we find that a parabolic expression of the form

$$q_s = a(u_* - u_t)^2 \tag{4.5}$$

fits the data better than Eq. (4.4), as can be seen in Fig. 7 and in particular in the inset. In the limit $u_* >> u_t$ one obtains the classical behavior of Bagnold [31], as verified by the dash-dotted line in Fig. 7 and which is consistent with Refs. [32–35]. The limit $u_* \approx u_t$, however, yields the quadratic relation for the flux given in Eq. (4.5). Physically this is due to the fact that close to u_t the laminar component is relevant.

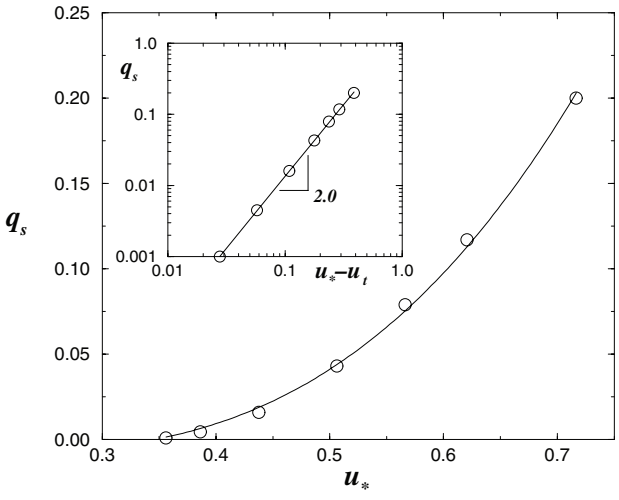

Fig. 7. Plot of the saturated flux q_s as function of u_*. The dashed line is the fit using the expression proposed by Lettau and Lettau [32], $q_s \propto u_*^2(u_* - u_t)$, with $u_t = 0.35 \pm 0.02$. The full line corresponds to Eq. (4.5) and the dashed-dotted line to Bagnold's relation, $q_s \propto u_*^3$ [31]. The results shown in the inset confirm the validity of the the power-law relation Eq. (4.5), $q_s \propto (u_* - u_t)^2$. The critical point is $u_t = 0.33 \pm 0.01$.

5 Conclusion and outlook

We have found [16] that although the distribution of channel widths in a porous medium made by a two-dimensional RSA process is rather complex and exhibits a crossover at $l \sim D$, the distribution of fluxes through these channels shows an astonishingly simple behavior, namely a square-root stretched exponential distribution that scales in a simple way with the porosity. Future tasks consist in generalizing these studies to higher Reynolds numbers, other types of disorder and three dimensional models of porous media.

We also presented results for the inertial capture of particles in two-dimensional periodic as well as random porous media [26]. For the periodic model in the absence of gravity, there exists a finite Stokes number below which particles never get trapped. Furthermore, our results indicate that the transition from non-trapping to trapping with the Stokes number is of second order with a scaling exponent $\alpha \approx 0.5$. In the presence of gravity, we show that (*i*) this non-trapping regime is suppressed (i.e., $St_c = 0$) and (*ii*) the scaling exponent changes to $\alpha \approx 1$. We intend to investigate in the future the possibility of non-trapping at first contact and the effect on the capture efficiency of simultaneous multiple particle release.

We finally also showed results of simulations [41] giving insight about the layer of granular transport in a turbulent flow. The lack of experimental noise allows for a precise study close to the critical threshold velocity u_t that lead us to a parabolic dependence of the saturated flux. The present model can be extended in many ways including the study of the dependence of the aeolian transport layer on the grain diameter, the gas viscosity, and the solid or fluid densities. This would allow to calculate, for instance, the granular transport on Mars and compare with the expression presented in the literature [35].

We thank the Max Planck Prize for financial support.

References

1. S.L. Soo, *Particles and Continuum: Multiphase Fluid Dynamics* (Hemisphere, New York, 1989)
2. D. Gidaspow, *Multiphase Flow and Fluidization* (Academic Press, San Diego, 1994)
3. K. Pye, H. Tsoar, *Aeolian sand and sand dunes* (Unwin Hyman, London, 1990)
4. F.A.L. Dullien, *Porous Media – Fluid Transport and Pore Structure* (Academic, New York, 1979)
5. P.M. Adler, *Porous Media: Geometry and Transport* (Butterworth-Heinemann, Stoneham MA, 1992)
6. M. Sahimi, *Flow and Transport in Porous Media and Fractured Rock* (VCH, Boston, 1995)
7. FLUENT (trademark of FLUENT Inc.) is a commercial package for computational fluid dynamics
8. S.N. Coppersmith, C.-h. Liu, S. Majumdar, O. Narayan, T.A. Witten, Phys. Rev. E **53**, 4673 (1996)
9. A. Canceliere, C. Chang, E. Foti, D.H. Rothman, S. Succi, Phys. Fluids A **2**, 2085 (1990)
10. S. Kostek, L.M. Schwartz, D.L. Johnson, Phys. Rev. B **45**, 186 (1992)
11. N.S. Martys, S. Torquato, D.P. Bentz, Phys. Rev. E **50**, 403 (1994)
12. J.S. Andrade Jr., D.A. Street, T. Shinohara, Y. Shibusa, Y. Arai, Phys. Rev. E. **51**, 5725 (1995)
13. A. Koponen, M. Kataja, J. Timonen, Phys. Rev. E **56**, 3319 (1997)
14. S. Rojas, J. Koplik, Phys. Rev. E **58**, 4776 (1998)
15. J.S. Andrade Jr., U.M.S. Costa, M.P. Almeida, H.A. Makse, H.E. Stanley, Phys. Rev. Lett. **82**, 5249 (1999)
16. A.D. Araújo, W.B. Bastos, J.S. Andrade Jr., H.J. Herrmann, Phys. Rev. E, physics/0511085 (accepted)
17. H. Marshall, M. Sahraoui, M. Kaviany, Phys. Fluids **6**, 507 (1993)
18. S. Torquato, *Random Heterogeneous Materials: Microstructure and Macroscopic Properties* (Springer, New York, 2002)
19. G.V. Voronoi, J. Reine Angew. Math. **134**, 198 (1908)
20. D.F. Watson, Comp. J. **24**, 167 (1981)
21. C. Tien, *Granular Filtration of Aerosols and Hydrosols* (Butterworths, Boston, 1989)
22. C. Ghidaglia, L. de Arcangelis, J. Hinch, E. Guazzelli, Phys. Rev. E **53**, R3028 (1996); Phys. Fluids **8**, 6 (1996)

23. J. Lee, J. Koplik, Phys. Fluids **13**, 1076 (2001)
24. D.L. Koch, R.J. Hill, Annu. Rev. Fluid Mech. **33**, 619 (2001)
25. D.E. Rosner, P. Tandon, Chem. Eng. Sci. **50**, 3409 (1995)
26. A.D. Araújo, J.S. Andrade Jr., H.J. Herrmann (preprint)
27. H. Marshall, M. Sahraoui, M. Kaviany, Phys. Fluids **6**, 507 (1993)
28. R.A. Bagnold, *The Physics of Blown Sand and Desert Dunes* (Methuen, London, 1941)
29. R.S. Anderson, M. Sørensen, B.B. Willetts, Acta Mech. (Suppl.) **1**, 1 (1991)
30. H.J. Herrmann, in *The Physics of Granular Media*, edited by H. Hinrichsen, D. Wolf (Wiley VCH, Weinheim, 2004), p. 233-252
31. R.A. Bagnold, Proc. R. Soc. Lond A **167**, 282 (1938)
32. K. Lettau, H. Lettau, in *Exploring the World's Driest Climate*, edited by H. Lettau, K. Lettau, Center for Climatic Research (Univ. of Wisconsin, Madison, 1978)
33. P.R. Owen, J. Fluid Mech. **20**, 225 (1964)
34. M. Sørensen, in *Proc. Int. Wkshp. Physics of Blown Sand*, Vol. 1 (Univ. of Aarhus, Denmark, 1985), p. 141; Acta Mech. (Suppl.) **1**, (1991) 67
35. B.R. White, Geophys. Res. **84**, 4643 (1979)
36. G.R. Butterfield, in *Turbulence: Perspectives on Flow and Sediment Transport*, edited by N.J. Cliffod, J.R. French, J. Hardisty, Chapter 13 (John Wiley, 1993), p. 305
37. K. Nishimura, J.C.R. Hunt, J. Fluid. Mech. **417**, 77 (2000)
38. J.E. Ungar, P.K. Haff, Sedimentology **34**, 289 (1987)
39. B. Andreotti, J. Fluid Mech. **510**, 47 (2004)
40. P. Nalpanis, J.C.R. Hunt, C.F. Barrett, J. Fluid Mech. **251**, 661–685 (1993)
41. M.P. Almeida, J.S. Andrade Jr., H.J. Herrmann, Phys. Rev. Lett. **96**, 018001 (2006)
42. L. Prandtl, in *Aerodynamic Theory*, edited by W.F. Durand, Vol. 3 (Springer, Berlin, 1935), p. 34
43. R.S. Anderson, P.K. Haff, Science **241**, 820 (1988)
44. F. Rioual, A. Valance, D. Bideau, Phys. Rev. E **62**, 2450–2459 (2000)